Supplement of Atmos. Chem. Phys., 26, 8809–8838, 2026
https://doi.org/10.5194/acp-26-8809-2026-supplement

Atmospheric Chemistry and Physics
Open Access
EGU

Supplement of

Reassessment of the glyoxal-to-formaldehyde ratio R_{GF} as a proxy for VOC source identification

Simon Bittner et al.

Correspondence to: Simon Bittner (simon.bittner@uni-bremen.de)

S1 Fit settings

Table S1. Fit settings for NO_2 vis for Orléans, Athens, and Incheon.

Fit parameter		Selection/source
Spectral range		425 nm – 490 nm
Polynomial degree		6
Wavelength calibration		Solar atlas from Chance and Kurucz (2010)
Reference		Closest two zenith-sky spectra in time interpolated to time of measurement
Cross-section	Temperature	Data source
O_3	223 K	Serdyuchenko et al. (2014) with I_0 correction
NO_2	294 K, 220 K	Vandaele et al. (1996) with I_0 correction
O_4	293 K	Thalman and Volkamer (2013)
H_2O	296 K	Rothman et al. (2010)
Ring	-	Computed by QDOAS, Danckaert et al. (2017)

Table S2. Fit settings for NO_2 UV for Orléans, Athens, and Incheon.

Fit parameter		Selection/source
Spectral range		338 nm – 370 nm
Polynomial degree		6
Wavelength calibration		Solar atlas from Chance and Kurucz (2010)
Reference		Closest two zenith-sky spectra in time interpolated to time of measurement
Cross-section	Temperature	Data source
O_3	223 K, 243 K	Serdyuchenko et al. (2014) with I_0 correction
NO_2	294 K, 220 K	Vandaele et al. (1996) with I_0 correction
BrO	223 K	Fleischmann et al. (2004)
HCHO	298 K	Meller and Moortgat (2000)
O_4	293 K	Finkenzeller and Volkamer (2022)
Ring	-	Computed by QDOAS with and without Pukite Terms, Danckaert et al. (2017)

Table S3. Fit settings HCHO for Orléans, Athens, and Incheon.

Fit parameter		Selection/source
Spectral range		337.5 nm – 361 nm
Polynomial degree		6
Wavelength calibration		Solar atlas from Kurucz et al. (1984)
Reference		Closest zenith-sky spectrum in time
Cross-section	Temperature	Data source
HCHO	298 K	Meller and Moortgat (2000)
O_3	223 K	Serdyuchenko et al. (2014)
NO_2	294 K	Vandaele et al. (1996)
O_4	293 K	Thalman and Volkamer (2013)
Ring	-	Computed by QDOAS, Danckaert et al. (2017)

Table S4. Fit settings CHOCHO for Orléans, Athens, and Incheon.

Fit parameter		Selection/source
Spectral range		436 nm – 470 nm
Polynomial degree		6
Wavelength calibration		Solar atlas from Kurucz et al. (1984)
Reference		Closest two zenith-sky spectra in time interpolated to time of measurement
Cross-section	Temperature	Data source
CHOCHO	296 K	Volkamer et al. (2005)
O_3	223 K	Serdyuchenko et al. (2014)
NO_2	294 K, 220 K	Vandaele et al. (1996)
O_4	293 K	Thalman and Volkamer (2013)
H_2O	293 K	Rothman et al. (2013)
Ring	-	Computed by QDOAS, Danckaert et al. (2017)

S2 Data filtering thresholds

Table S5. Station specific thresholds used for data filtering. Valid datapoints fulfil the listed criteria.

	ATTO	Orléans
RMS	< 0.001	< 0.001
Intensity (vis)	$> 5 \times 10^4\,\mathrm{counts\,s^{-1}}$	$> 5 \times 10^4\,\mathrm{counts\,s^{-1}}$
Intensity (UV)	$> 1 \times 10^4\,\mathrm{counts\,s^{-1}}$	$> 1 \times 10^4\,\mathrm{counts\,s^{-1}}$
SZA	$< 80\,^\circ$	$< 80\,^\circ$
rel. Error	$< 50\,\%$	$< 50\,\%$
	Incheon	Athens
RMS	< 0.001	< 0.001
Intensity (vis)	$> 5 \times 10^4\,\mathrm{counts\,s^{-1}}$	–
Intensity (UV)	$> 3 \times 10^3\,\mathrm{counts\,s^{-1}}$	–
SZA	$< 80\,^\circ$	$< 80\,^\circ$
rel. Error	$< 50\,\%$	$< 50\,\%$

S3 Detailed results of statistic tests

Table S6. Statistical test results for environment differences (Welch t-test) and site-to-site differences (Welch ANOVA).

Test	Data	Aggregation	Logarithmic	Value	p value	$p < 0.05$
Welch t-test	(ATT+Orl)–(Ath+Inc)	monthly mean	yes	$t = -5.8$	8×10^{-8}	yes
Welch ANOVA	all stations	monthly mean	yes	$F = 19$	3×10^{-8}	yes

Table S7. Post-hoc Games–Howell test results for pairwise station comparisons.

Pair	Aggregation	Logarithmic	Value	p value	$p < 0.05$
ATTO–Orléans	monthly mean	yes	0.16	6.7×10^{-2}	no
ATTO–Athens	monthly mean	yes	-0.15	3.2×10^{-2}	yes
ATTO–Incheon	monthly mean	yes	-0.31	2.5×10^{-5}	yes
Orléans–Athens	monthly mean	yes	-0.32	7.4×10^{-5}	yes
Orléans–Incheon	monthly mean	yes	-0.47	1.7×10^{-7}	yes
Athens–Incheon	monthly mean	yes	-0.15	6.1×10^{-2}	no

Table S8. Welch t-test results for weekday vs. weekend differences.

Station	Data	Aggregation	Logarithmic	t statistic	p value	$p < 0.05$
ATTO	weekday–weekend	weekly mean	no	-0.3	8×10^{-1}	no
Orléans	weekday–weekend	weekly mean	no	-0.2	8×10^{-1}	no
Athens	weekday–weekend	weekly mean	no	4.4	2×10^{-5}	yes
Incheon	weekday–weekend	weekly mean	no	2.7	8×10^{-3}	yes

Table S9. Seasonal and annual median absolute uncertainties of R^*_{GF} for all stations (ATTO scaled). ATTO seasons follow tropical definitions. The values in brackets are the 25%- and 75% percentile.

		ATTO		Orléans	Athens	Incheon
Annual		0.38 (0.27–0.60) %		0.64 (0.42–1.05) %	0.58 (0.41–0.90) %	0.91 (0.68–1.19) %
	DJ (transition)	0.51 (0.35–0.75) %	DJF (winter)	1.51 (1.08–2.19) %	1.06 (0.79–1.49) %	1.21 (1.05–1.48) %
	FMAM (wet)	0.56 (0.41–0.85) %	MAM (spring)	0.84 (0.56–1.33) %	0.69 (0.49–0.98) %	0.96 (0.75–1.21) %
	JJ (transition)	0.33 (0.24–0.46) %	JJA (summer)	0.51 (0.36–0.75) %	0.42 (0.33–0.53) %	0.75 (0.56–0.97) %
	ASON (dry)	0.29 (0.23–0.40) %	SON (autumn)	0.58 (0.32–1.10) %	0.76 (0.57–1.08) %	0.90 (0.68–1.14) %

S4 Supporting figures

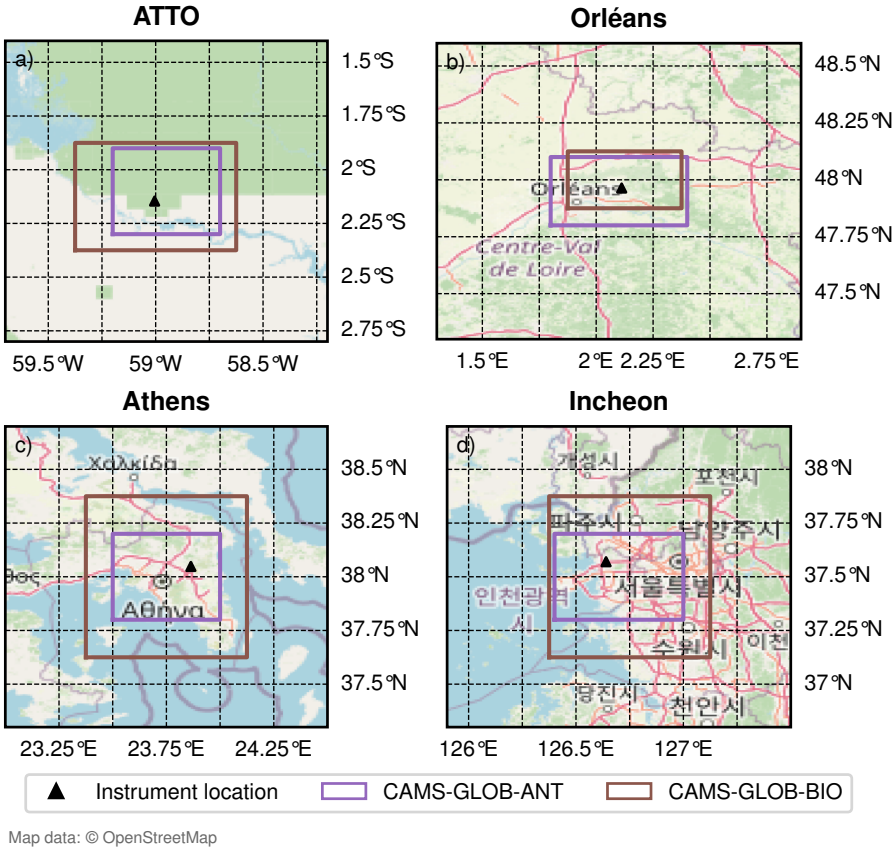

Figure S1. Maps of all four sites showing the considered area for computing the average anthropogenic CAMS emissions (purple) and the average biogenic CAMS emissions (brown).

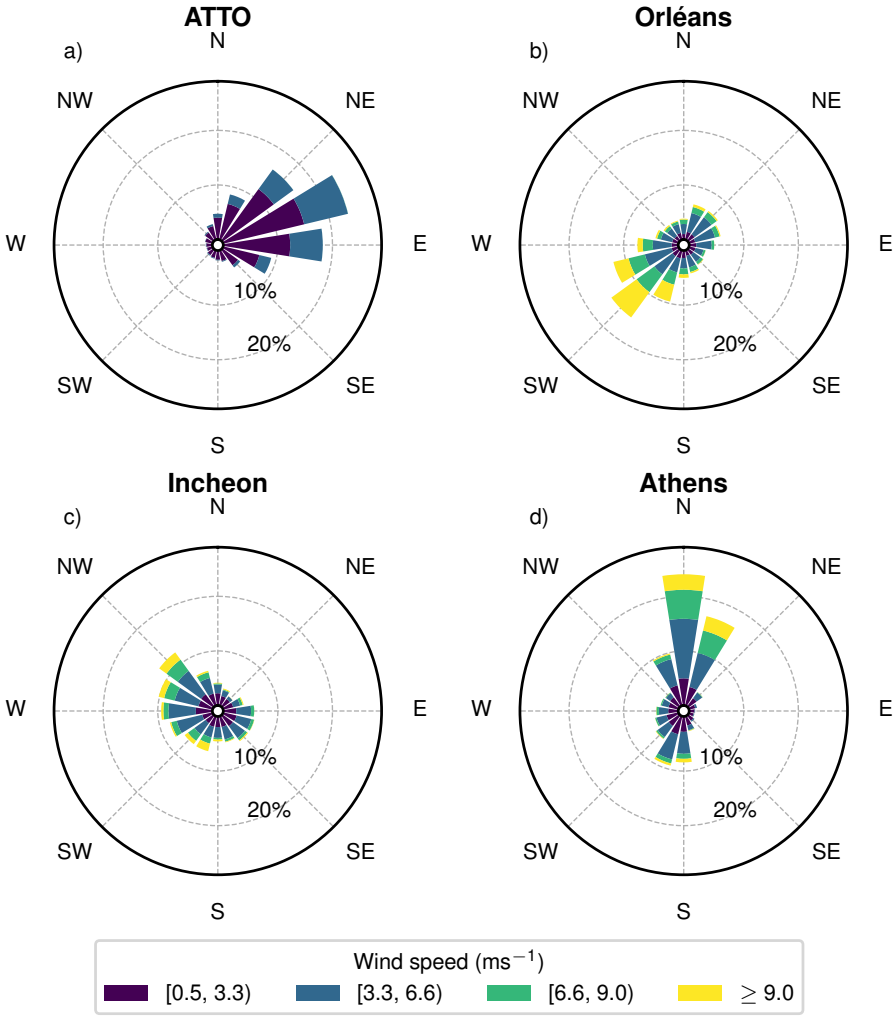

Figure S2. Wind roses showing the prevailing wind directions and wind speed in percentage during the respective measurement period for ATTO a), Orléans b), Incheon c) and Athens d). The bars show the percentage of wind direction from that direction and the colour indicates the wind speed.

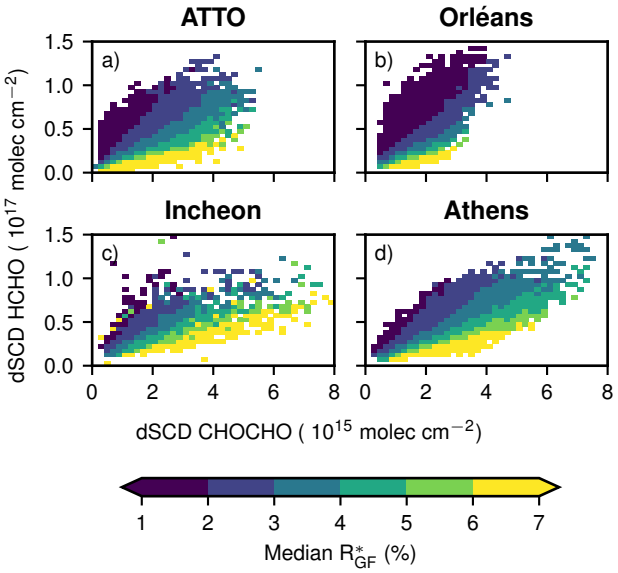

Figure S3. Median R^*_{GF} values for different bins of CHOCHO dSCDs and HCHO dSCDs.

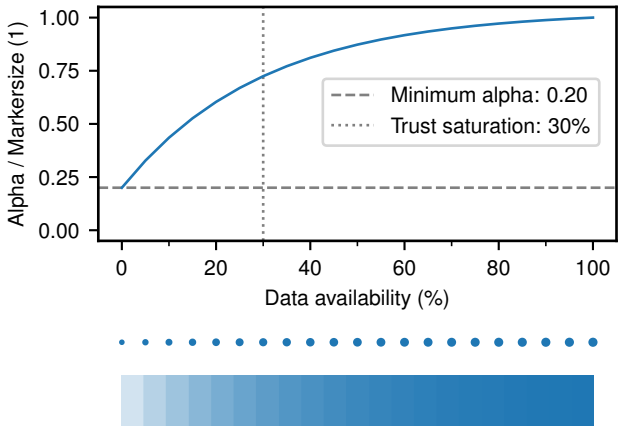

Figure S4. Applied mapping to show data availability as alpha or marker size. The data availability is defined per panel, i.e. the bin with highest number of measurements in that panel is taken as 100%. The mapping corresponds to $f(x) = \alpha_{\min} + (\alpha_{\max} - \alpha_{\min})(1 - \exp(-\frac{x}{f_0}))(1 - \exp(-\frac{1}{f_0}))^{-1}$ with $\alpha_{\min} = 0.2$, $\alpha_{\max} = 1$, $f_0 = 0.3$.

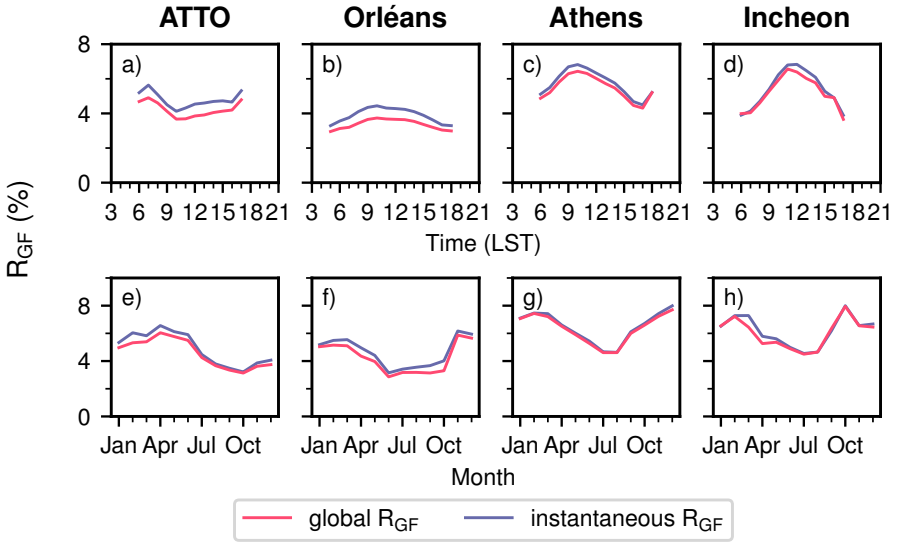

Figure S5. Visualization of the different averaging approaches using the 10:00 local solar time bin from the diurnal cycle of Orléans. The distributions of CHOCHO dSCD (top) and of HCHO dSCD (bottom) are shown on the left, with the respective mean indicated with the red vertical line. On the right, the distribution of R_{GF} and the instantaneous R_{GF} (purple vertical line) as well as the global R_{GF} (red vertical line) is shown.

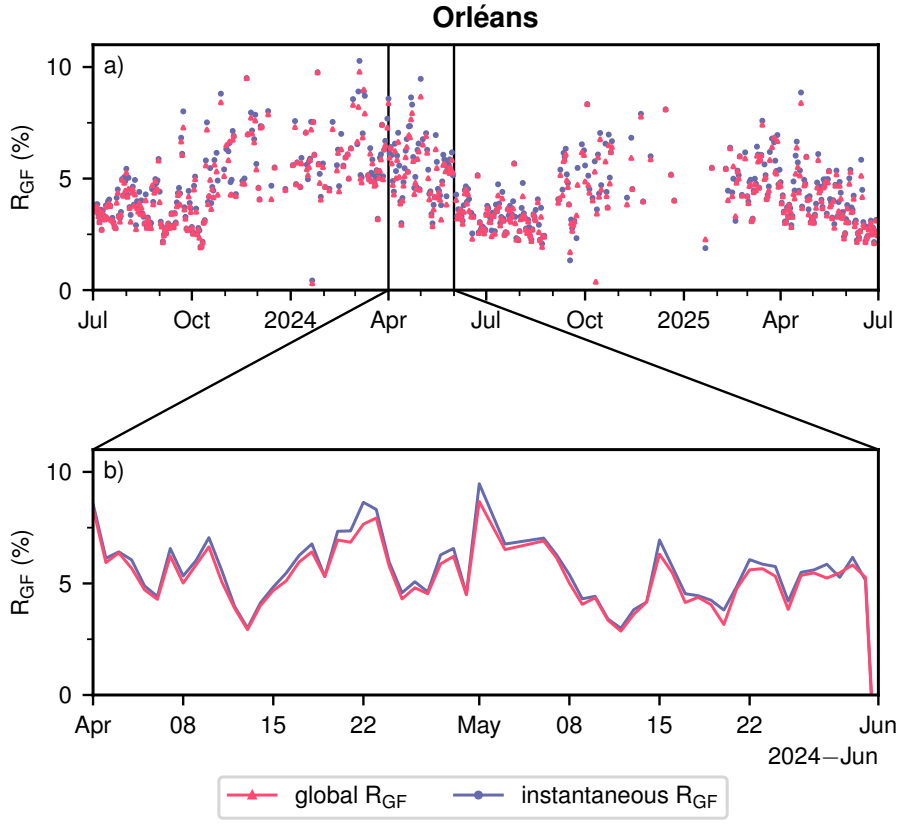

Figure S6. Timeseries of global R_{GF} and instantaneous R_{GF} for daily means at Orléans. Panel a) shows the whole measurement period. Panel b) shows a zoomed-in period.

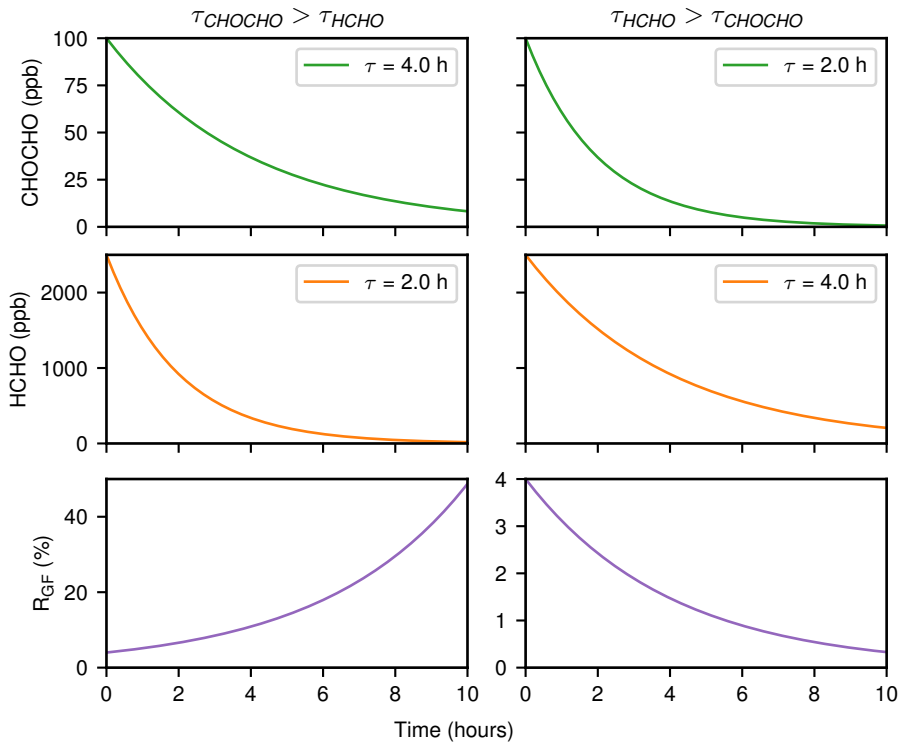

Figure S7. Simplified R_{GF} sensitivity to differences in chemical lifetime assuming an exponential decay.

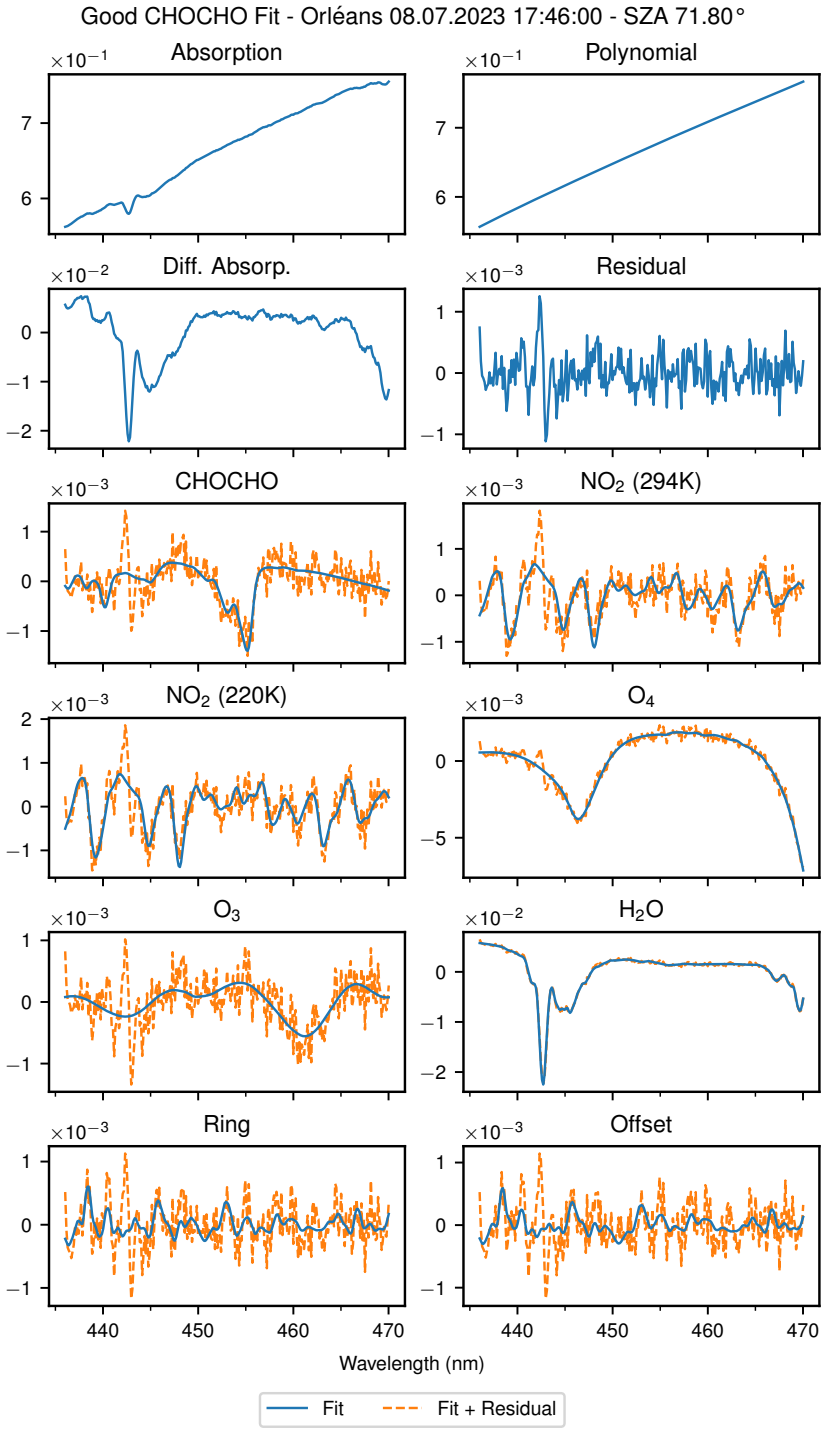

Figure S8. Fit components of a good CHOCHO fit in Orléans. The blue line indicates the fit and the dashed orange line indicates the residual added to the fit.

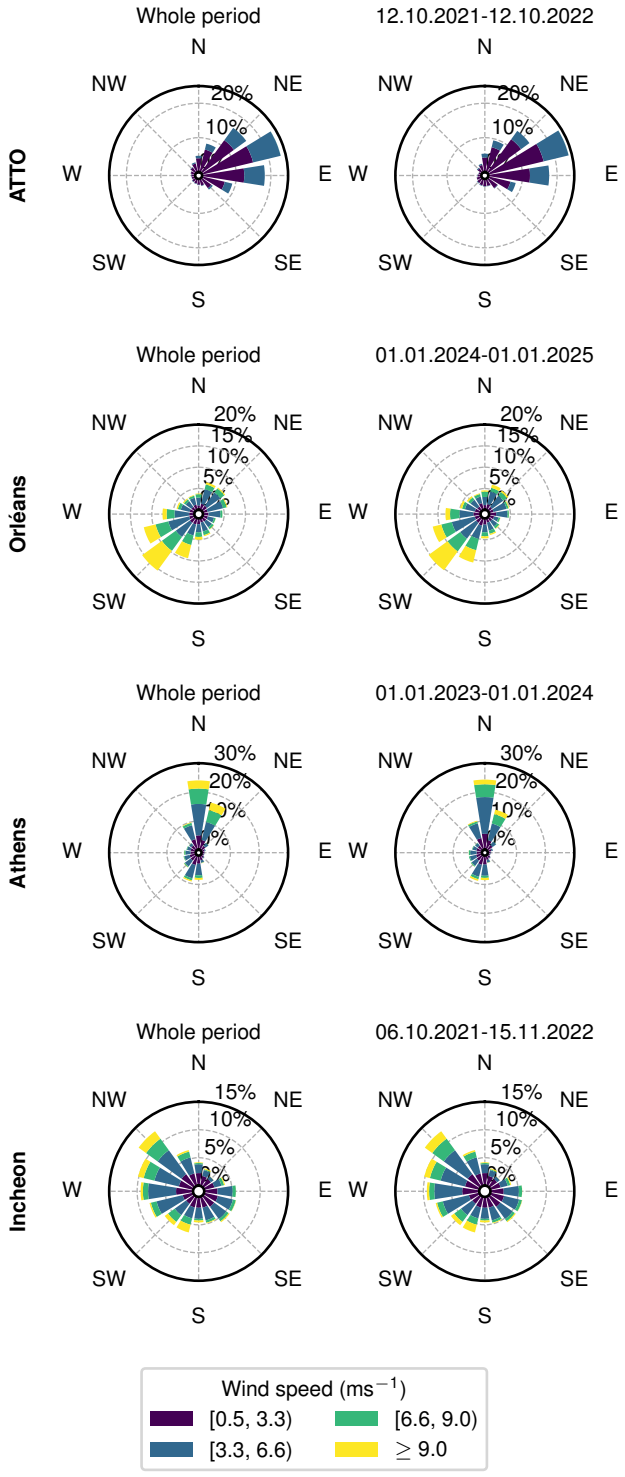

Figure S9. Wind rose of the whole measurement period and the wind rose of the subperiod that is selected for the backward trajectory runs.

S5 R_{GF} via VCDs from 30 ° viewing elevation

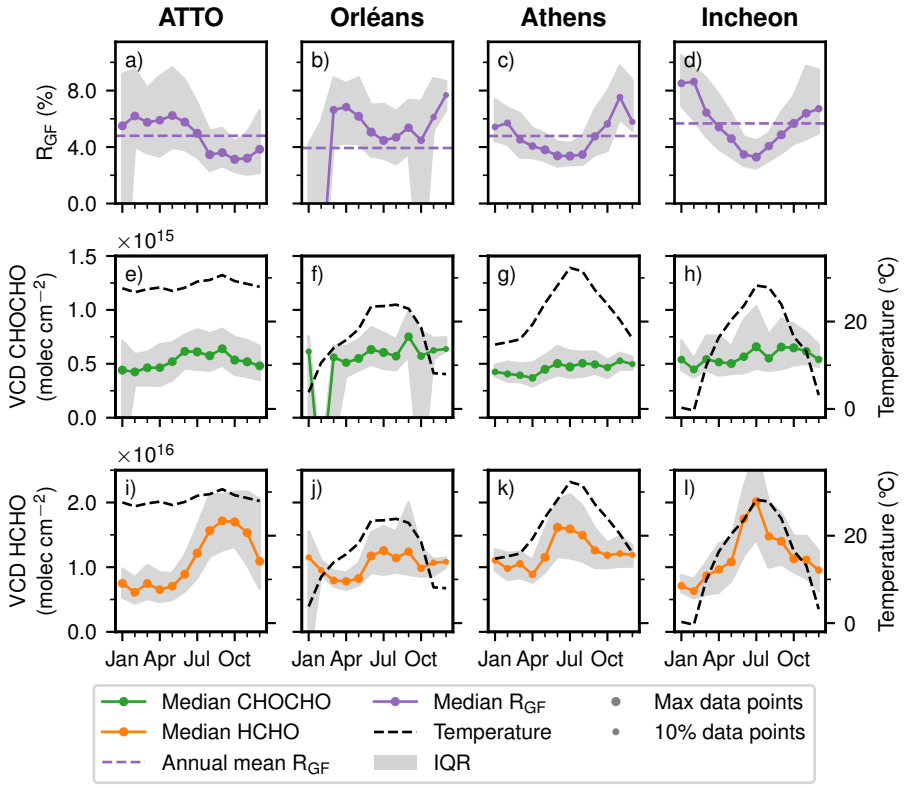

Figure S10. Seasonal cycle of R_{GF} without O_4 correction (top row), CHOCHO VCDs (centre row), HCHO VCDs (bottom row) for ATTO, Orléans, Athens, and Incheon. Marker size scales with the number of contributing observations, with smaller markers indicating fewer measurements. The VCDs are approximated by using the 30 ° viewing elevation. Panels e) and i) are are self-created based on Donner (2024).

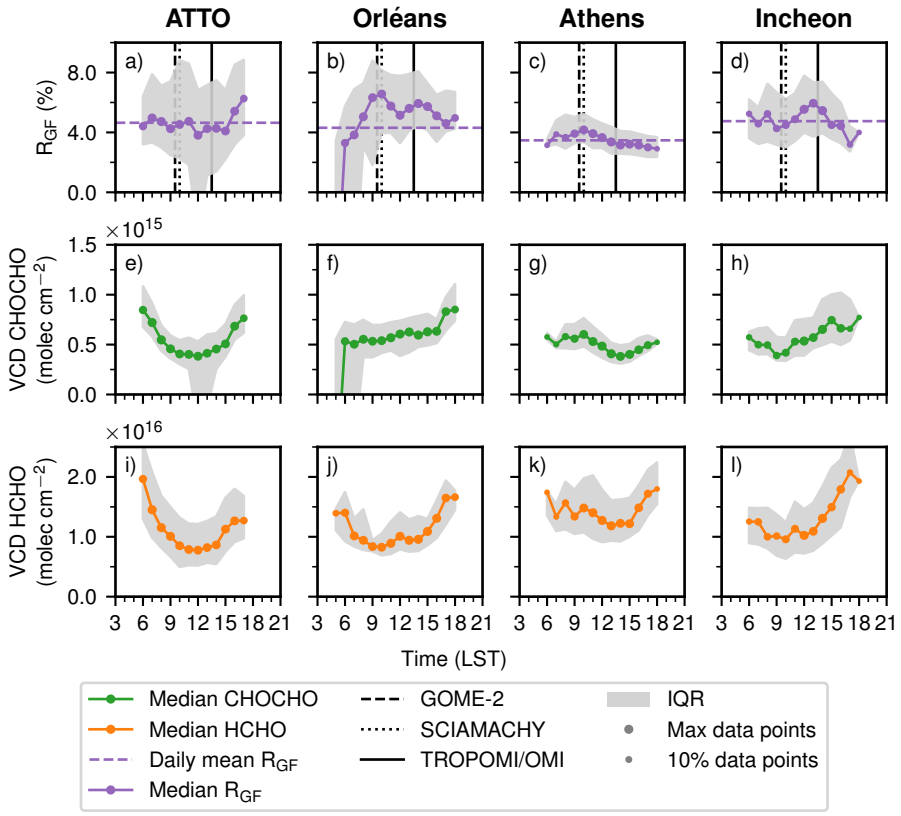

Figure S11. Diurnal cycle of R_{GF} without O_4 correction (top row), CHOCHO VCDs (centre row), HCHO VCDs (bottom row) for ATTO, Orléans, Athens, and Incheon. Marker size scales with the number of contributing observations, with smaller markers indicating fewer measurements. The VCDs are approximated by using the 30° viewing elevation. Panels e) and i) are are self-created based on Donner (2024).

S6 R_{GF} without O_4 correction

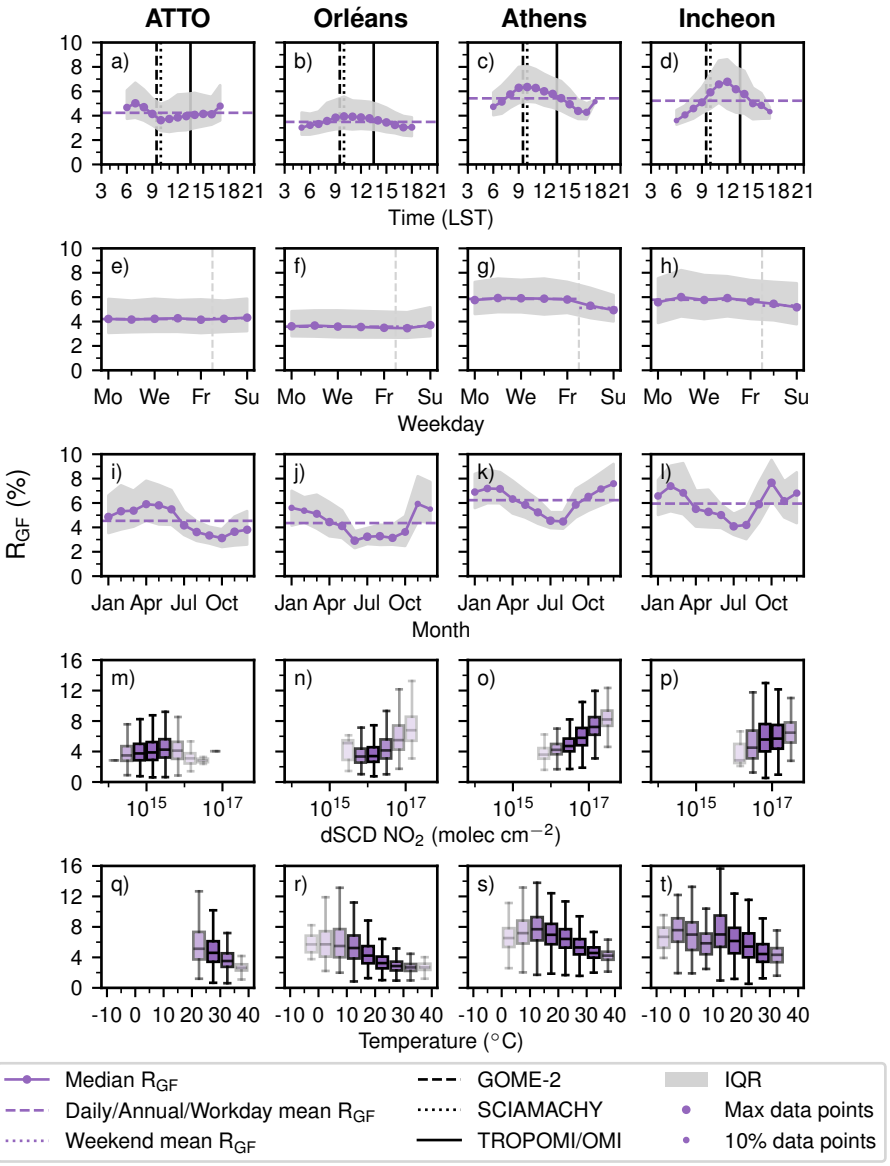

Figure S12. Overview of all main figures of the study for R_{GF} (without O_4 correction). Within each box, the horizontal line indicates the median and the box spans the IQR; whiskers extend to 1.5 IQR. Box transparency scales with the number of contributing measurements, with more transparent boxes indicating fewer observations. Missing box plots indicate that no data points fall within that interval.

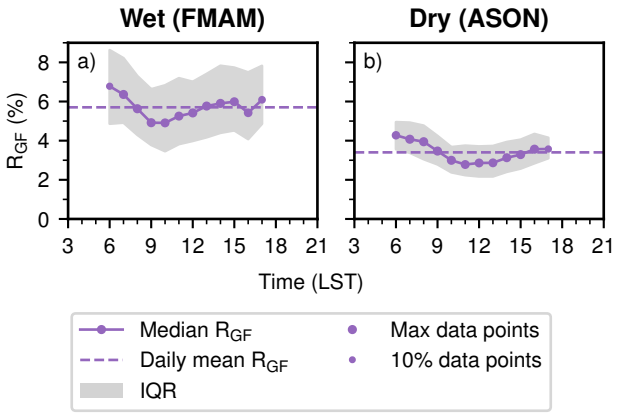

Figure S13. Diurnal cycles in the wet a) and dry b) season of R_{GF} (without O_4 correction) at ATTO. Marker size scales with the number of contributing observations, with smaller markers indicating fewer measurements.

S7 O_4 ratio scaling for ATTO

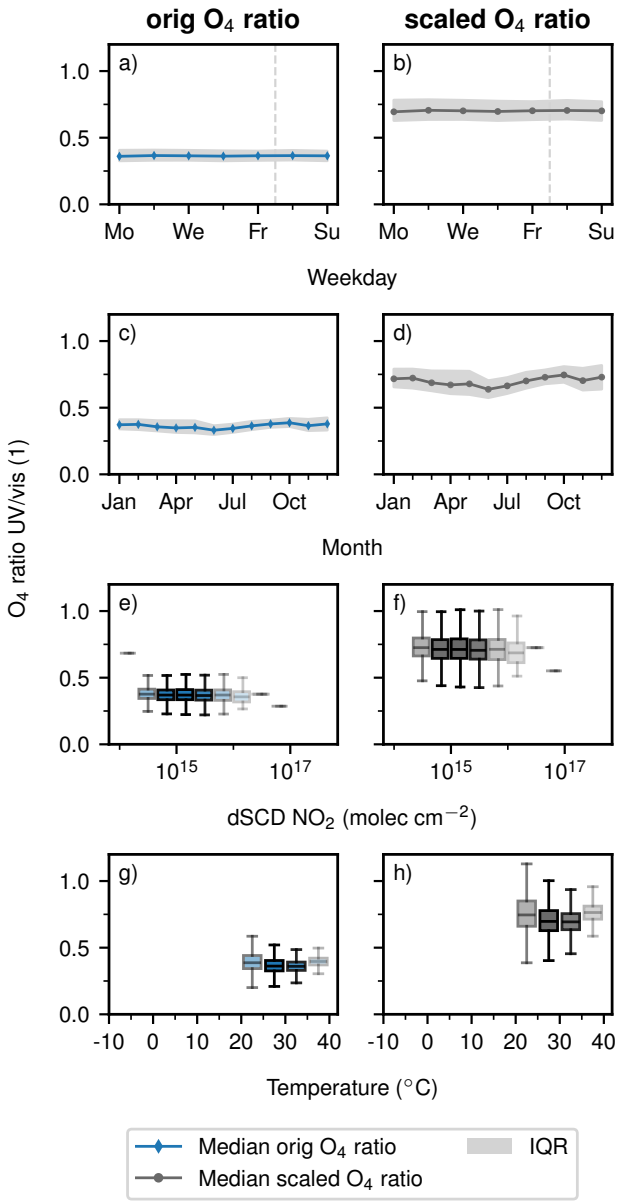

Figure S14. Overview of the behaviour of the O_4 ratio with and without scaling the O_4 vis dSCDs for ATTO. Within each box, the horizontal line indicates the median and the box spans the IQR; whiskers extend to 1.5 IQR. Box transparency scales with the number of contributing measurements, with more transparent boxes indicating fewer observations. Missing box plots indicate that no data points fall within that interval.

References

Chance, K. and Kurucz, R.: An improved high-resolution solar reference spectrum for earth's atmosphere measurements in the ultraviolet, visible, and near infrared, Journal of Quantitative Spectroscopy and Radiative Transfer, 111, 1289–1295, https://doi.org/10.1016/j.jqsrt.2010.01.036, 2010.

Danckaert, T., Fayt, C., van Roozendael, M., de Smedt, I., Letocart, V., Merlaud, A., and Pinardi, G.: QDOAS Software user manual - Version 3.2, Royal Belgian Institute for Space Aeronomy, https://uv-vis.aeronomie.be/software/QDOAS/QDOAS_manual.pdf, last access: 10 March 2026, 2017.

Donner, S.: Retrieving vertical profiles and tropospheric columns of formaldehyde from global long-term MAX-DOAS measurements, Ph.D. thesis, Johannes Gutenberg-Universität Mainz, https://doi.org/10.25358/OPENSCIENCE-11085, 2024.

Finkenzeller, H. and Volkamer, R.: O_2–O_2 CIA in the gas phase: Cross-section of weak bands, and continuum absorption between 297–500 nm, Journal of Quantitative Spectroscopy and Radiative Transfer, 279, 108 063, https://doi.org/https://doi.org/10.1016/j.jqsrt.2021.108063, 2022.

Fleischmann, O. C., Hartmann, M., Burrows, J. P., and Orphal, J.: New ultraviolet absorption cross-sections of BrO at atmospheric temperatures measured by time-windowing Fourier transform spectroscopy, Journal of Photochemistry and Photobiology A: Chemistry, 168, 117–132, https://doi.org/10.1016/j.jphotochem.2004.03.026, 2004.

Kurucz, R. L., Furenlid, I., Brault, J., and Testerman, L.: Solar flux atlas from 296 to 1300 nm, National Solar Observatory Atlas No. 1, 1984.

Meller, R. and Moortgat, G. K.: Temperature dependence of the absorption cross sections of formaldehyde between 223 and 323 K in the wavelength range 225–375 nm, Journal of Geophysical Research: Atmospheres, 105, 7089–7101, https://doi.org/10.1029/1999jd901074, 2000.

Rothman, L., Gordon, I., Barber, R., Dothe, H., Gamache, R., Goldman, A., Perevalov, V., Tashkun, S., and Tennyson, J.: HITEMP, the high-temperature molecular spectroscopic database, Journal of Quantitative Spectroscopy and Radiative Transfer, 111, 2139–2150, https://doi.org/10.1016/j.jqsrt.2010.05.001, 2010.

Rothman, L., Gordon, I., Babikov, Y., Barbe, A., Chris Benner, D., Bernath, P., Birk, M., Bizzocchi, L., Boudon, V., Brown, L., Campargue, A., Chance, K., Cohen, E., Coudert, L., Devi, V., Drouin, B., Fayt, A., Flaud, J.-M., Gamache, R., Harrison, J., Hartmann, J.-M., Hill, C., Hodges, J., Jacquemart, D., Jolly, A., Lamouroux, J., Le Roy, R., Li, G., Long, D., Lyulin, O., Mackie, C., Massie, S., Mikhailenko, S., Müller, H., Naumenko, O., Nikitin, A., Orphal, J., Perevalov, V., Perrin, A., Polovtseva, E., Richard, C., Smith, M., Starikova, E., Sung, K., Tashkun, S., Tennyson, J., Toon, G., Tyuterev, V., and Wagner, G.: The HITRAN2012 molecular spectroscopic database, Journal of Quantitative Spectroscopy and Radiative Transfer, 130, 4–50, https://doi.org/10.1016/j.jqsrt.2013.07.002, 2013.

Serdyuchenko, A., Gorshelev, V., Weber, M., Chehade, W., and Burrows, J. P.: High spectral resolution ozone absorption cross-sections - Part 2: Temperature dependence, Atmospheric Measurement Techniques, 7, 625–636, https://doi.org/10.5194/amt-7-625-2014, 2014.

Thalman, R. and Volkamer, R.: Temperature dependent absorption cross-sections of O_2-O_2 collision pairs between 340 and 630 nm and at atmospherically relevant pressure, Physical Chemistry Chemical Physics, 15, 15 371–15 381, https://doi.org/10.1039/c3cp50968k, 2013.

Vandaele, A. C., Hermans, C., Simon, P. C., Roozendael, M. V., Guilmot, J. M., Carleer, M., and Colin, R.: Fourier transform measurement of NO_2 absorption cross-section in the visible range at room temperature, Journal of Atmospheric Chemistry, 25, 289–305, https://doi.org/10.1007/bf00053797, 1996.

Volkamer, R., Spietz, P., Burrows, J., and Platt, U.: High-resolution absorption cross-section of glyoxal in the UV–vis and IR spectral ranges, Journal of Photochemistry and Photobiology A: Chemistry, 172, 35–46, https://doi.org/10.1016/j.jphotochem.2004.11.011, 2005.